Contents lists available at ScienceDirect

Nuclear Inst. and Methods in Physics Research, A

journal homepage: www.elsevier.com/locate/nima

Development of the digital multichannel analyzer for liquid scintillation detection

Yu-Jie Zhou [a,1], Chun-Hui Gong [a,1], Man-Li He [c], Pin Gong [b,d], Xiao-Bin Tang [b,d], Peng Wang [a,b,*], Yi Yang [a,**]

[a] *Jiangsu Key Laboratory of Chemical Pollution Control and Resources Reuse, School of Environmental and Biological Engineering, Nanjing University of Science and Technology, Nanjing, 210094, China*
[b] *Key Laboratory of Nuclear Technology Application and Radiation Protection in Astronautics (Nanjing University of Aeronautics and Astronautics), Ministry of Industry and Information Technology, China*
[c] *Department of General Education, Army Engineering University of PLA, Nanjing, 211101, China*
[d] *Department of Nuclear Science & Engineering, Nanjing University of Aeronautics and Astronautics, Nanjing, 210016, China*

ARTICLE INFO

ABSTRACT

The new digital multichannel analyzer (DMCA) based on field programmable gate array (FPGA) technology is successfully developed, and it is used for liquid scintillation detection. The performance of this system has been evaluated. The analog signal output emanating from the photomultiplier tube (PMT) is transformed into digital signals through the utilization of an amplifier and a high-speed analog-to-digital converter (ADC). Information about the energy, timing, and pulse shape characteristics of the radiation event is contained in the digital signal. Subsequently, this digital signal is directed towards the FPGA for digital signal processing. In order to reduce the thermal and electronic noise, the dual-channels configuration and the signal coincidence function are added to DMCA for optimizing the validity of signal. The signal coincidence unit is designed within the FPGA, optimizing the synchronization of signals. The measurement data is transmitted to a computer via USB interface. The energy spectra of gamma sources, namely ^{22}Na, ^{60}Co, and ^{137}Cs, as well as the alpha source ^{232}Th, were measured utilizing the newly developed system. Notably, thermal and electronic noise interference is reduced in the coincidence measurement mode, and the coincidence energy spectra are improved compared to the singles measurement. In contrast to commercially available systems, the advantages of our design in terms of miniaturization, cost-effectiveness, and expandability are demonstrated.

1. Introduction

With the development of nuclear technology, the potential hazards associated with radioactive contamination have been raised. For example, the life and health of the public have been severely affected by the waste liquid from nuclear facilities and Fukushima nuclear wastewater [1,2]. Therefore, the advancement of liquid radioactivity measurement technology assumes paramount significance in the domains of radioactive contamination prevention, control, and the progression of nuclear technology. Efficient liquid scintillation detection methods should be used for the measurement of liquid radioactivity due to the severe self-absorption and low activity concentrations in radioactive liquids [3–5]. In the liquid scintillation detection method, the measurement sample is mixed directly with the liquid scintillator. Potential interference due to self-absorption effect is effectively mitigated by liquid scintillation detection method. The liquid scintillation detection method has high counting efficiency (up to 100%). Although it is a conventional radiometric technique, but still a competitive technique for the measurement of many radionuclides [6].

Conventional liquid scintillation detection systems depend on analog electronic modules, which exhibit suboptimal integration, significant physical bulkiness, and high energy-consumption. In recent years,

---

digital pulse processing has been used as a viable alternative to traditional analog electronic modules in the field of nuclear physics instrumentation. It opens new possibilities for pulse shape analysis. The parallel computing capabilities inherent in field programmable gate array (FPGA) have positioned them as an ideal solution for high-performance digital signal processing. The hardware design of the digital multichannel analyzer (DMCA) is simplified by the acquisition and digital signal processing system using FPGA chip, reducing its power consumption and cost [7,8]. Currently, there are many research groups actively investigating and developing the DMCA hardware system to replace conventional analog modalities [9–14]. If only a single PMT is used in the liquid scintillation detection methods, there will be a high background level for the 0–2000 keV counting region. This high background is normally due to the background noise (thermal noise and electronic background noise) and the large amplification factor from the PMT. The instrument background signal is detrimental to the evaluation of low activity samples and low-energy radionuclides [15]. Two PMT and a coincidence module are used to differentiate background signals from true nuclear decay events in the scintillation vial, which is referred to as coincidence measurement [15–18]. In particular, it is important to note that coincidence measurement is able to distinguish between instrumental background and nuclear decay events, but is unable to deal with environmental radiation effects.

In this study, an online coincidence measurement DMCA system based on FPGA technology was successfully developed, specifically tailored for liquid scintillation detection. To verify the performance of the newly developed system, tests were conducted encompassing gamma-ray and alpha-ray radiation measurements. Standard radioactive sources and liquid scintillator were employed during the assessment, which encompassed single-channel as well as dual-channel coincidence tests. This paper delves into the details of the design and performance evaluation of our DMCA system.

2. Materials and methods

Three main components are comprised in the new system, namely, a detection module, a portable power source, and a DMCA board based on FPGA technology. The connection between the detection module and the DMCA board is established through a bayonet nut connector (BNC). The block diagram illustrating the architecture of the newly developed dual-channel DMCA system designed specifically for liquid scintillation

detection is shown in Fig. 1. The research and design of the various components of the new system will be elaborated in the subsequent sections of this paper.

2.1. Detection module design

The detection module for liquid scintillation detection is arranged in a dark housing, in order to further avoid light leakage and outside interference. The detection module encompasses an optical chamber, two compact photomultiplier tubes (PMT), a scintillation vial and two dedicated negative high-voltage power supply units. The size and geometry of the detection module components are shown in Fig. 2(a). For this study, Hamamatsu H11934-100 square package type PMT is employed, which possess a total of 12 dynode stages. These PMT are characterized by their compact dimensions (30mmx30mm), broad spectral range (300–650 nm), and rapid response time (7.1 ns). The PMT operated at a standard working voltage of −900 V, and for their power supply, we utilized compact negative high-voltage modules. The portable power source was responsible for providing the power to the two compact negative high-voltage modules. The use of miniaturized PMT means that the effective light collection area is reduced. In order to improve the light collection efficiency, the design of the optical chamber needs to be carefully considered. Previously, optical chambers were mainly made of metal materials, and the inner walls were painted with a highly reflective paint. Recent studies have focused on incorporating diffuse reflective materials into optical chambers, with polytetrafluoroethylene (Teflon) emerging as a frequently employed material in these studies [19,20]. In view of weight and cost considerations, the optical chamber in the design is constructed using white Teflon material, chosen specifically for its ability to ensure a high level of diffuse reflection efficiency. In order to avoid the light trapping caused by internal reflection, the acute angle of the inner wall of the optical chamber were chamfered. Two PMT are arranged symmetrically on both sides of the optical chamber as light collection components for coincidence measurements, as shown in Fig. 2(b).

2.2. Dual-channel DMCA board design

A dual signal channels DMCA board (Fig. 3) has been developed based on FPGA chip. This DMCA board is used for digital signal processing, and enables precise coincidence measurement of the output
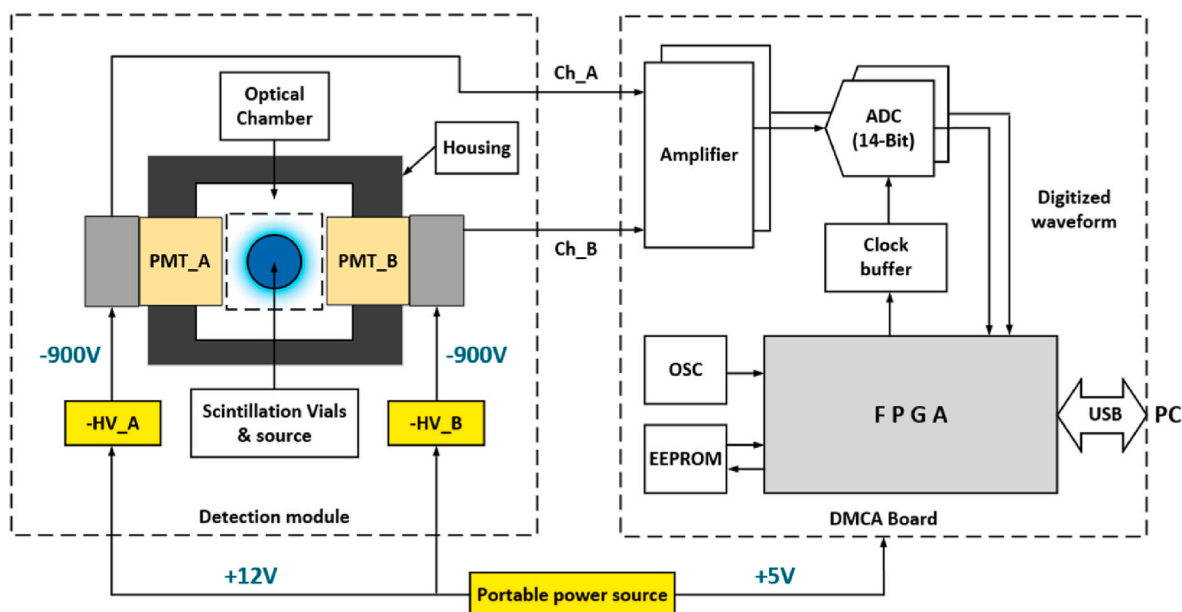

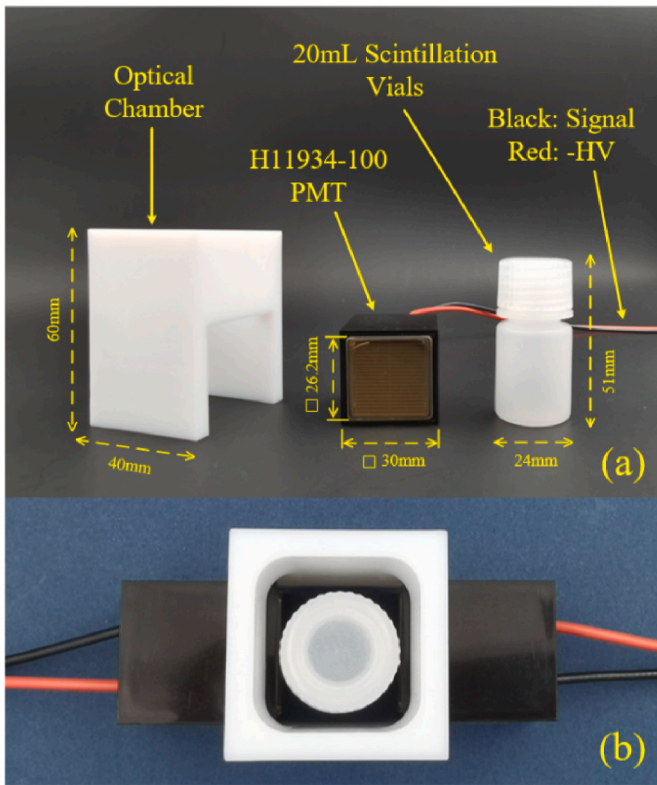**Fig. 1.** Block diagram of the new system.

Fig. 2. Photographs of detection module components. (a) Size and geometry of the components. (b) Layout of PMT and optical chamber in the detection module.
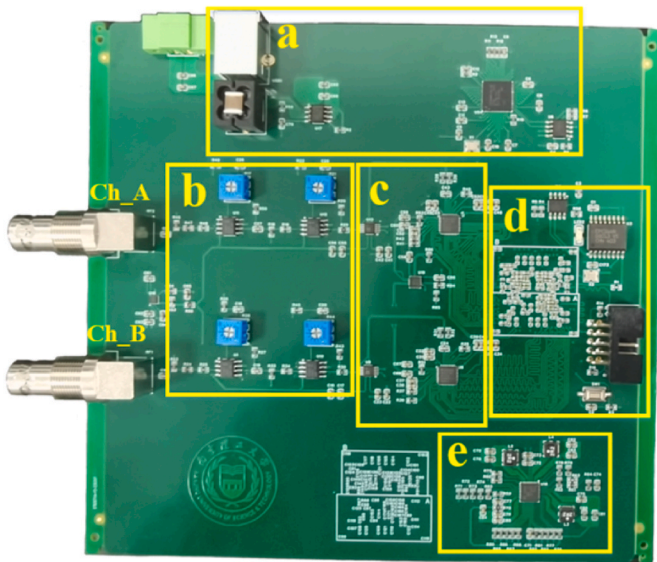

Fig. 3. Photograph of the newly developed DMCA board: (a) USB; (b) Amplifiers; (c) ADC; (d) FPGA; (e) Integrated power management.

signals from the detection module. An FPGA chip of Altera Cyclone IV series was used with a working frequency of 50 MHz. To ensure optimal clock signal quality, an oscillator (OSC) was employed to generate the clock signal, and a global clock network was established using a phase locked loop (PLL). The signals from the two channels of the detection module are initially processed by a two-stage amplifier analog circuit. The output signals of PMT and amplifier are shown in Fig. 4. The PMT signal is amplified and shaped by the amplifier to have an extended
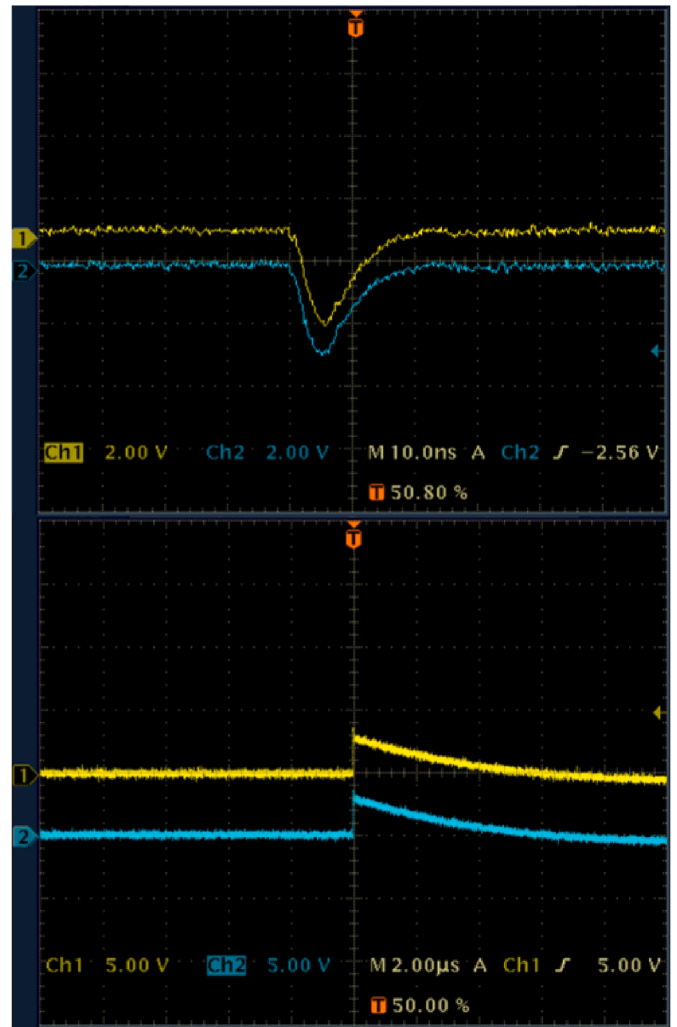

Fig. 4. The output signal of PMT (top). The output signal of amplifier (bottom). (There is a voltage offset between the two channels in order to discriminate two channel pulses).

decay time for analog-to-digital converter (ADC) processing and subsequent digital signal processing. Meanwhile, negative pulses are converted to positive pulses. Subsequently, the signals are sampled using a 14-bit ADC (Analog Devices AD9649) operating at a sampling rate of 80 MHz. The signal is accurately digitized by this high-resolution ADC, and preservation of the essential information for further analysis and processing. The parallel digital signal outputted by the ADC is directed to the FPGA for further processing. The JTAG interface and logic analyzer are employed to facilitate the reading and analysis of signals from individual modules within the FPGA, which is convenient for subsequent debugging and upgrading of the system. The data and status information of the DMCA are transmitted to a computer via a USB port.

The DMCA board is designed to work with +5 V power supply (+3 to +5.5 V is acceptable), and it can also be powered by USB port. The amplifiers are supplied with ±5 V, and the FPGA core voltage and peripheral device voltages are provided by an integrated power management chip. The comprehensive power consumption of the system has been measured to approximate 2.04 W.

2.3. FPGA logic and coincidence method

A range of essential functions for signal conditioning and analysis are included in the FPGA-based online digital signal processing module. This module includes signal adjustment, dual-channel digital filtering,

trigger logic, amplitude extraction, pile-up rejection, energy analysis, and coincidence logic. Digital signals are processed in real-time and efficiently by these integrated processing capabilities. To consider that the two channels may have different time responses due to detector reaction time, signal wire length and other uncertainties, an input signal delay unit is added to the signal adjustment module. The faster signal is delayed several cycles to match the slower one. This meticulous synchronization process ensures accurate and consistent signal processing, potential discrepancies due to different channel response times are mitigated. The diagram of the FPGA logic design is shown in Fig. 5.

FPGA has limited internal logical resources, 226 multipliers and 3.888Mbits embedded memory in total are available. Therefore, high-order finite impulse response (FIR) digital filter is impossible to realize in the FPGA. In order to address the challenges posed by limited FPGA resources, an infinite impulse response (IIR) digital filter is employed for the purpose of filter shaping. The complexity of the system design is effectively reduced, and the FPGA logic is optimized. Prior to the trigger event, the cusp-like pulse shaping technique is applied to the original pulse waveform. The impact of noise is mitigated by this shaping process, thereby improving the overall signal quality. Equations (1)–(5) are difference equations of cusp-like pulse shaping:

$$d^k(n) = x(n) - x(n-k) \tag{1}$$

$$d^1(n) = x(n) - x(n-1) \tag{2}$$

$$p(n) = p(n-1) + d^k(n) - kd^1(n-l) \tag{3}$$

$$q(n) = q(n-1) + m_2 p(n) \tag{4}$$

$$s(n) = s(n-1) + q(n) + m_1 p(n) \tag{5}$$

Where k and l are delay parameters, $k = 2l + 1$. The duration of the rising and falling edges in the cusp-like pulse shaping process is determined by these parameters. The parameters m_1 and m_2 are interdependent gain parameters for pulse shaping, $m_1/m_2 = 1/(e^{Ts/\tau}-1)$, The parameter Ts represents the sampling period of the ADC, and τ denotes the time constant associated with the falling edge of the original pulse waveform. The baseline is stabilized after the cusp-like pulse shaping, which helps to eliminate false triggers. Moreover, the falling edge of the waveform becomes steep, and baseline recovery time is reduced. Then the accuracy of pulse localization is improved, and the pile-up of events is reduced.

An event trigger is generated when the amplitude of the shaped waveform, represented by the series $s(n)$, surpasses a predetermined threshold level.

In order to enhance the signal-to-noise ratio (SNR) and facilitate precise signal amplitude extraction for energy calculation, trapezoidal pulse shaping is employed. It is also implemented with IIR digital filter. Equations (6)–(9) are difference equations of trapezoidal pulse shaping:

$$y_1(n) = x(n) - x(n-n_b) \tag{6}$$

$$y_2(n) = y_2(n-1) + \frac{y_1(n) - dy_1(n-1)}{n_a} \tag{7}$$

$$y_3(n) = y_3(n-1) + y_2(n-1) \tag{8}$$

$$y_4(n) = y_3(n) - y_3(n-n_b) \tag{9}$$

Where $d = e^{-Ts/\tau}$, $n_a = t_a/Ts$, $n_b = t_b/Ts$. The parameter t_a represents the duration of the rising edge of the trapezoid waveform, while t_b corresponds to the combined duration of the rising edge and the flat top region of the trapezoid waveform. The amplitude of the trapezoid-shaped signal, which is proportional to the incident radiation energy. It is calculated by subtracting the average of the baseline from the average of the top platform. Fig. 6 shows an exemplary waveform obtained from the FPGA via a logic analyzer, the effects of the cusp-like filter and trapezoid filter are shown.

The timing diagram of coincidence logic and pile-up rejection within the FPGA is shown in Fig. 7. The trigger and coincidence management process in the FPGA operates as follows: The variable delay unit of the input signal is used to ensure an intentional time delay in channel B relative to channel A. A trigger pulse is generated when the amplitude of the signal following cusp-like pulse shaping exceeds the threshold. The operation of the coincidence unit and the pile-up rejection unit is initiated by a trigger pulse originating from channel A. A programmable coincidence window is included in the coincidence unit, and a coincidence flag pulse is generated when the trigger pulse occurs in both channel A and channel B within the coincidence window. The generated coincidence flag pulse is extended by the flat top time of the trapezoid waveform and serves as the coincidence signal, which is utilized for amplitude extraction when the trapezoidal waveform reaches a stable state. In the event of an unsuccessful coincidence, the pulse amplitude is not extracted. The trapezoidal signal generated by channel B is omitted
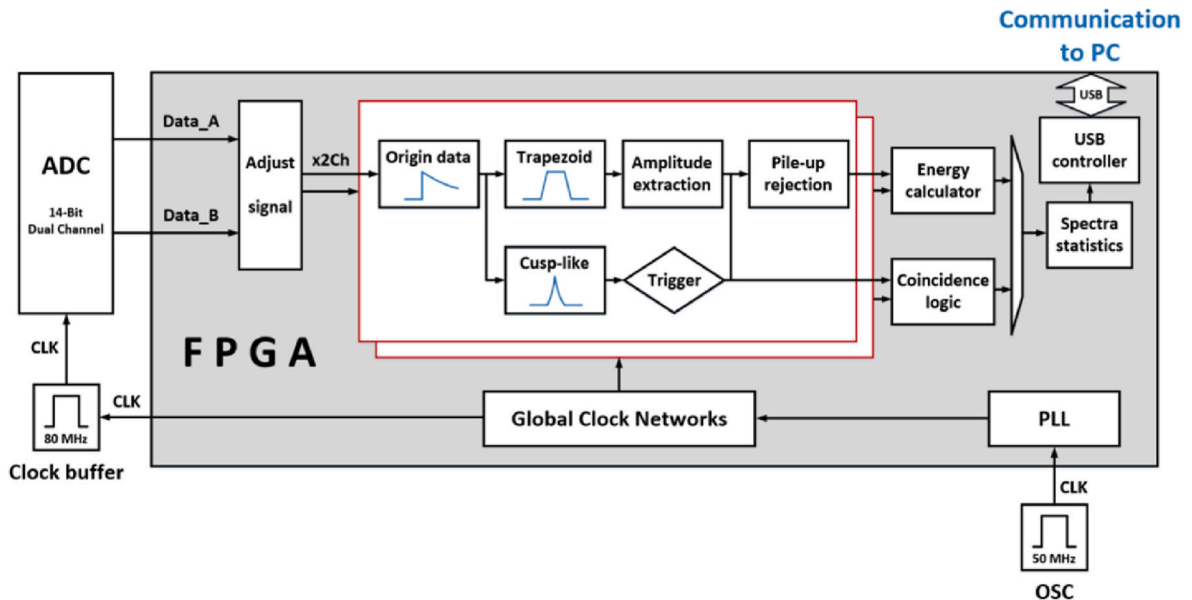

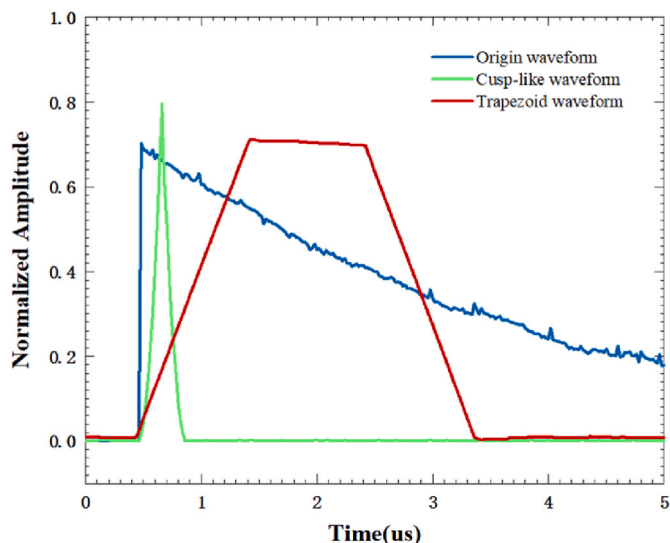
Fig. 5. Diagram of the FPGA logic design.

Fig. 6. Pulse waveform example collected from FPGA.

in Fig. 7. The pile-up event is generated by pulse signals that are very close to each other in the same signal channel, which leads to inaccuracies during amplitude extraction. A dead-time window that identifies the presence of successive triggers and generates a pile-up flag signal is contained in the pile-up rejection unit. In the presence of a pile-up flag signal, the extraction of pulse amplitude is bypassed, irrespective of a successful coincidence. This is due to the trapezoidal pulse amplitudes being overlapped during the pile-up events, resulting in inaccurate information regarding the energy spectrum. By deactivating the coincidence unit, a single-channel energy spectrum measurement can be obtained. The FPGA logic design was implemented using the Quartus II (13.0) development software.

2.4. Experimental setup

A photograph of the experimental setup along with a comprehensive block diagram illustrating the key components and their

interconnections are shown in Fig. 8. The liquid organic scintillator EJ-309 (Eljen Technology) was employed by the experimental setup. With a maximum emission wavelength of 424 nm, EJ-309 offers superior light output and scintillation efficiency. Notably, EJ-309 also possesses several advantageous features, including a high flash point, low vapor pressure, and low chemical toxicity. These features ensure the accurate and safe assessment of radioactivity levels. A 20 mL liquid scintillation vial was employed as a containment vessel for both the sample and liquid scintillator within the optical chamber. Two compact PMT were meticulously arranged in a symmetrical configuration, flanking the liquid scintillation vial with precision. The PMT is biased at −900 V, and the resulting anode output from each PMT is seamlessly directed to the DMCA board through the BNC connector, facilitating subsequent signal processing and analysis. The spectral measurements were performed employing radioactive sources, namely ^{22}Na, ^{60}Co, ^{137}Cs, and ^{232}Th. The spectrum data, obtained through the DMCA board, was efficiently transmitted to the computer system for subsequent visualization and analysis.

3. Results and discussion

3.1. Light collection

The optical chamber is an important component in the detection module to improve the efficiency of light collection. In order to determine the effectiveness of the light chamber. We measured the energy spectra of the ^{137}Cs source with and without the optical chamber, and the results are shown in Fig. 9. The solid red line in the figure shows the energy spectrum without optical chamber. The counts are shifted toward the low-energy part of the energy spectrum, and there is a large loss of counts in the high-energy part. This results in indistinct scattering peak and Compton edge. The black solid line is the energy spectrum with optical chamber. Scattering peak and Compton edge can be clearly observed in the energy spectrum, and the energy resolution is significantly improved. The optical chamber effectively solves the problem of reduced effective light collection area caused by miniaturized PMT. All subsequent energy spectrum measurements in the experiment will be with optical chamber.
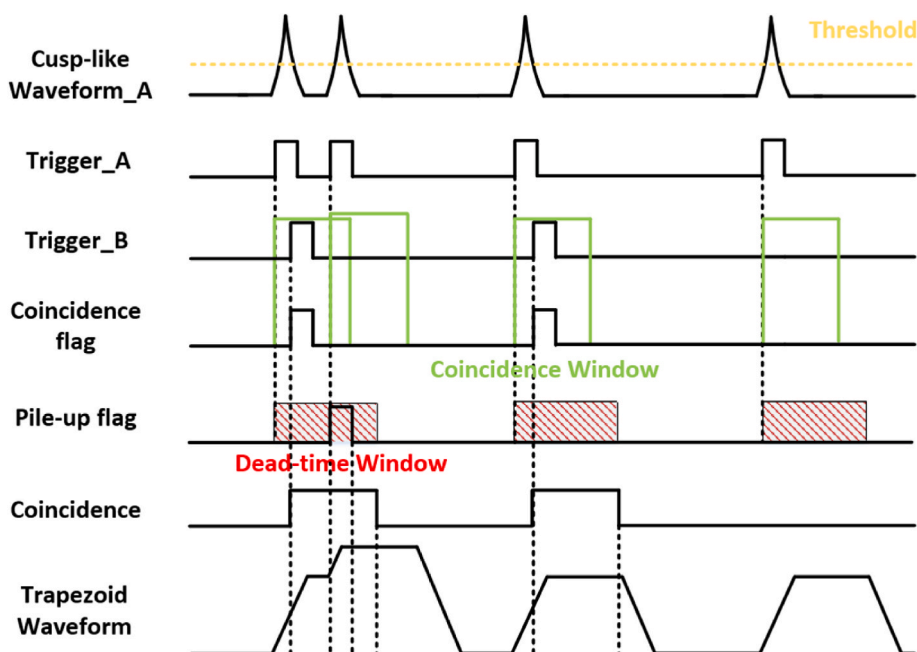

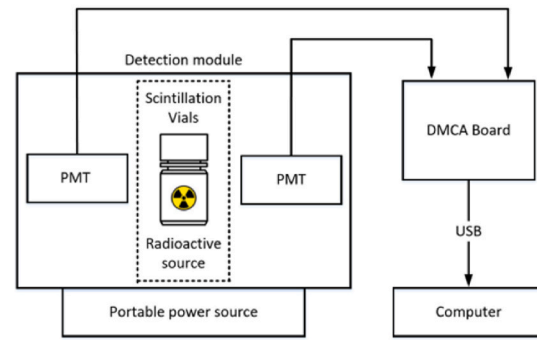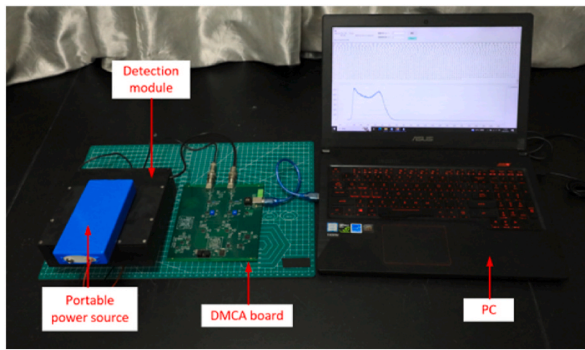**Fig. 7.** The timing diagram of the coincidence logic and pile-up rejection.

Fig. 8. A photo of the experimental equipment and the block diagram of the experimental setup.
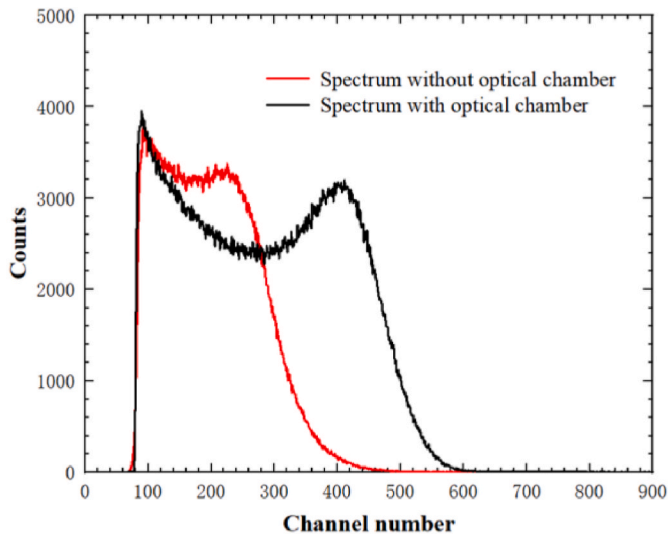

Fig. 9. Comparison of energy spectra obtained with optical chamber and without optical chamber using the ^{137}Cs source.

Fig. 10. DMCA response to voltage function generator.

3.2. Pulse linearity and energy calibration of DMCA

To ascertain the effective radiation energy detection capability of the DMCA, two distinct methods were employed to conduct testing and evaluation. First, a voltage function generator was used to evaluate the pulse linearity response of the DMCA. Pulses from 0 to 5.0 V, in steps of 0.1 V, produced by a function generator were input to the DMCA board, and the output signals in the channels were obtained. In Fig. 10 the correlation between the channel number and the input pulses voltage amplitude is shown, here is also included the linear fit whose correlation coefficient is 0.9999.

Moreover, standard gamma-ray sources including ^{22}Na, ^{60}Co, and ^{137}Cs were employed to calibrate the detection system. The calibration was performed by plotting the energy spectrum of each source. The constituents of the organic liquid scintillator primarily consist of carbon and hydrogen, characterized by their low atomic weight. Additionally, the photo-peak cross-section is very small for photon energies $E_\gamma \leq 3$ MeV. As a consequence, the light output distribution of gamma-ray for the organic liquid scintillator is mainly due to Compton scattered electrons. The recoil electron energy (E_c) corresponding to the Compton edge can be determined by a theoretical equation:

$$E_c = \frac{2E_\gamma^2}{m_0 c^2 + 2E_\gamma} \tag{10}$$

Where E_γ is the energy of the incident gamma-ray, and $m_0 c^2$ is the rest mass energy of electrons (0.511 MeV). In Table 1, the position of
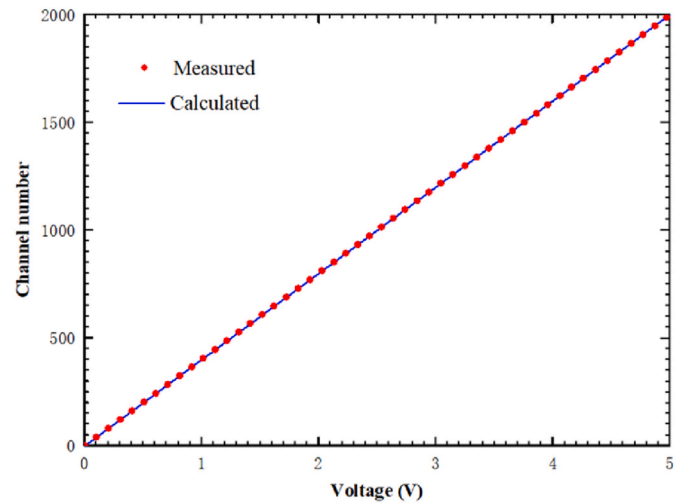
maximum of the Compton edges energy E_{max}, and maximum of the Compton electron energy E_c for standard ^{22}Na, ^{60}Co, and ^{137}Cs gamma-ray sources are shown.

The channel number at 75% of Compton edge maximum was used to calculate the calibration line [21]. The outcomes of the calibration process, including the energy spectra (light output) of ^{22}Na, ^{60}Co, and ^{137}Cs are shown in Fig. 11(a). Additionally, energy spectra were generated using the DT5781 (CAEN). The new system shows similar results to the energy spectrum obtained with DT5781. The obtained results enable the derivation of the gamma-ray response function for the DMCA, which is depicted in Fig. 11(b) and expressed as:

$$E_c = 1.2343 E_L - 59.516 \tag{11}$$

Where E_L is the light output, which equals the channel number. The correlation coefficient of the linear fit is 0.9997. The experimental error was included in the experimental data.

3.3. Timing calibration

In order to mitigate the inherent temporal disparity between the two

Table 1
E_γ, E_{max}, E_c of different gamma sources.

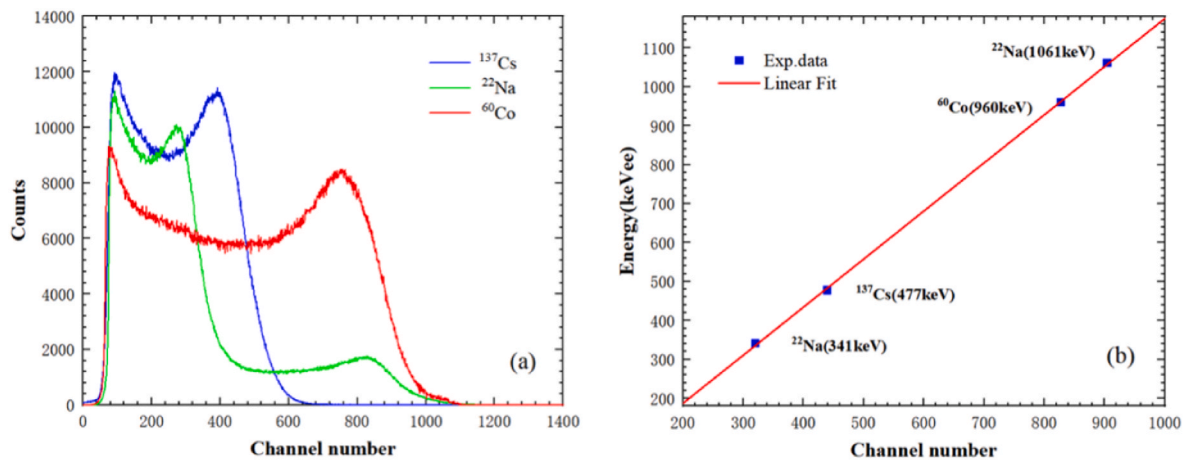| Source	E_γ/keV	E_{max}/keV	E_c/keV
^{22}Na	511	298	341
^{22}Na	1275	1012	1061
^{137}Cs	662	438	477
^{60}Co	1173	928	962

Fig. 11. (a) Energy spectra of ^{22}Na, ^{60}Co and ^{137}Cs. (b) Calibration line obtained from Compton edges of gamma-ray spectra.

signal channels on the DMCA board and guarantee the effective functioning of the coincidence unit, a meticulous timing calibration was conducted. A pulse function generator was employed to simultaneously stimulate both detectors within the coincidence measurement system, and a logic analyzer was used to determine the time differential between the two signal channels. A variable delay parameter has been incorporated into the signal adjustment module for one of the channels, with the purpose of achieving temporal synchronization between the two channels. The delay parameter is meticulously adjusted to harmonize the temporal sequence of the respective signals, thereby ensuring their concurrent arrival for subsequent processing and analysis. The inherent time difference between the two signal channels is less than 30 ns, with the timing resolution of the measurement being about 15 ns?

3.4. Coincidence measurement

Before the coincidence energy spectra measurement we measured the situation without scintillation vials. Background count levels in the 0–2000 keV counting region were obtained by reducing the threshold. The single PMT count rate without the coincidence module is about 11015 CPM (counts per minute). This is due to the thermal and electronic background noise as well as the large amplification factor from the PMT. Background count rates at different coincidence time were measured with the coincidence module turned on (The coincidence time corresponds to the width of the coincidence window). The coincidence count rates obtained are 45 CPM, 43 CPM, and 20 CPM under the condition that the coincidence time are 30 ns, 20 ns, and 10 ns? The instrumental background is effectively reduced, which is consistent with the description in Ref. [15].

The coincidence energy spectra of ^{137}Cs were measured by the dual-channel coincidence mode of the new system, allowing for a comparative analysis with single-channel energy spectra. The energy spectra of Channel_A and Channel_B in the coincidence and without coincidence modes were obtained. **The coincidence time were set to 30ns and 20ns.** The measurement outcomes are presented in Fig. 12. The coincidence energy spectra are improved compared to the singles measurement. Electron scattering peaks are more pronounced in the coincidence mode. **Notably, the time resolution of the setup is much larger than 10ns. Spectral distribution of 10ns coincidence time is distorted at low energies. Therefore the 20ns coincidence time is more appropriate to obtain a correct spectral shape and an optimal efficiency.**

Fig. 13 plots two-dimensional spectra where the abscissa and ordinate were pulse heights from channel_A and channel_B, respectively. The gradation in Fig. 13 indicates the number of events at a given position. The spectra were extended along the 45-deg line. Fig. 13(a) shows the two-dimensional spectra without coincidence and exhibits a large
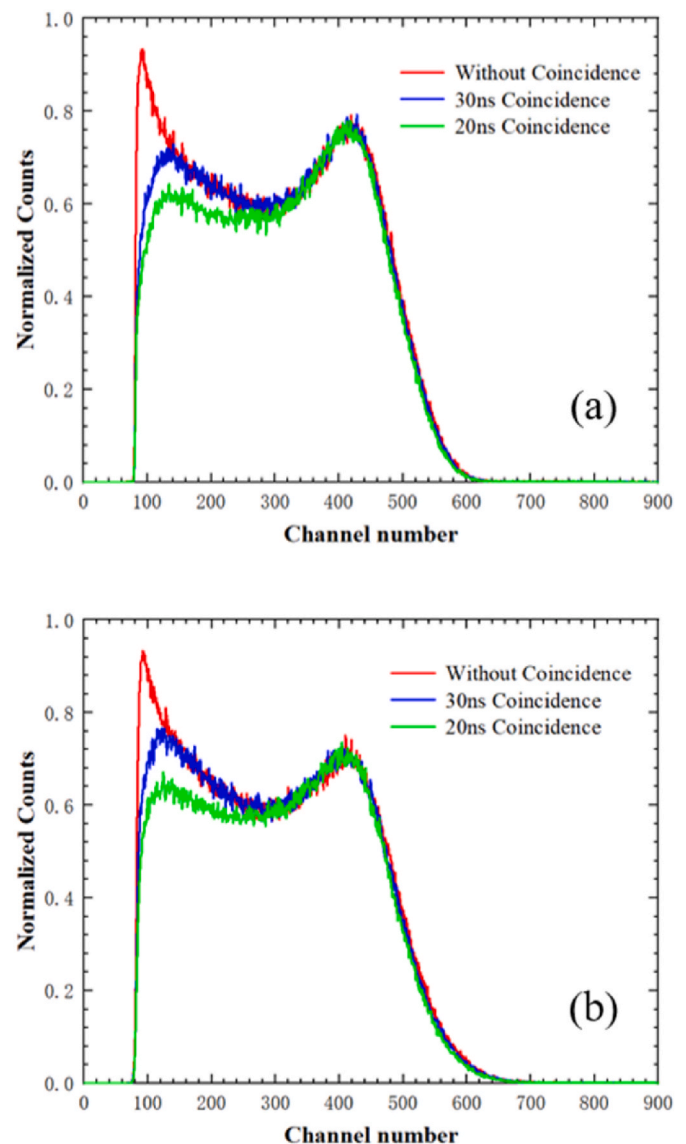

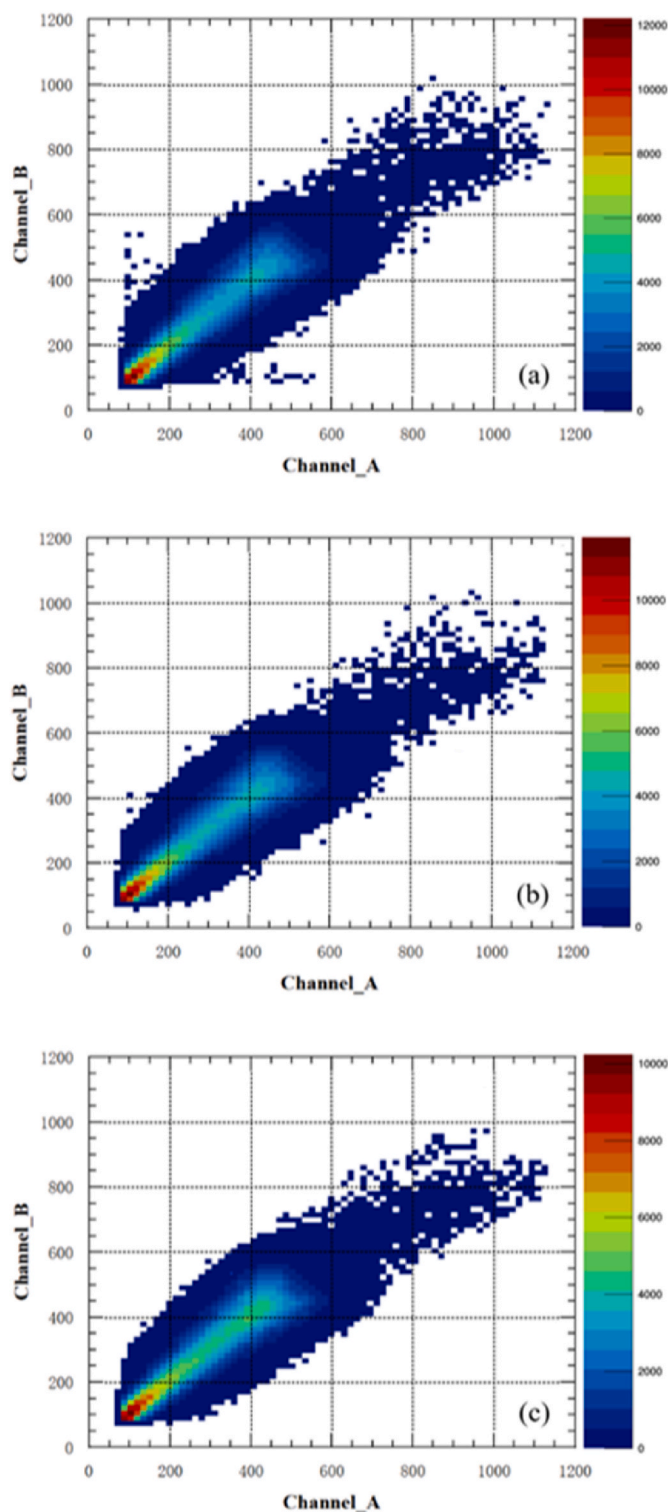**Fig. 12.** Spectra of ^{137}Cs source. (a) Channel_A; (b) Channel_B.

Fig. 13. Two-dimensional spectra of ^{137}Cs. (a) Without coincidence; (b) 30ns coincidence; (c) 20ns coincidence.

dispersion. Fig. 13(b) and (c) show the two-dimensional spectra with coincidence. As the coincidence time decreases, the dispersion of the two-dimensional spectra is reduced. The electron scattering peaks are more pronounced, which is consistent with the results of the one-dimensional spectra.

Additionally, the energy spectra of the pure alpha-emitting radionuclides ^{232}Th were subjected to measurement and analysis. Thorium (IV) nitrate hydrate was dissolved in distilled water, and three solutions

with concentrations of 0.2 mol/L, 0.1 mol/L, and 0.05 mol/L were prepared. For the preparation of ^{232}Th samples, 5 mL of each solution concentration was mixed with 15 mL of EJ-309 (Eljen Technology) liquid scintillator. Subsequently, the resulting mixtures were transferred into scintillation vials to serve as the ^{232}Th samples for further analysis and experimentation. The three ^{232}Th samples with varying concentrations were subjected to measurement using both the single-channel mode and the dual-channel coincidence mode. A consistent measurement time of 30 min was employed for all samples. Coincidence time was set to 20 ns? The results are shown in Fig. 14. It is noteworthy that the alpha-ray energy emitted during the decay of ^{232}Th is detected without any broadening of the spectrum due to energy deposition. In addition, the coincidence measurement mode suppresses instrumental background noise, which is advantageous for the detection of low activity and low energy samples. The performance of the novel DMCA system for liquid scintillation detection was validated.

Count rate of the γ and α measurements were recorded. The count rate at the same trigger threshold was obtained by calculating the spectrum counts with the real time. The two single channel count rate and the coincidence count rate for different radioactive sources are shown in Table 2. With coincidence time of 30ns and 20 ns, the coincidence count rate is reduced due to the decrease in coincidence time. But there is only a little difference between the count rates of the two single channels and the coincidence count rate. And the difference will be further reduced if the threshold is raised.

4. Conclusion

In this paper, a recently developed dual-channel DMCA system is presented, comprising a detection module and a DMCA board, as its central components. The system applies to the measurement of alpha and beta radioactivity in fluids. Two miniaturized PMT in the detection module are used for performing coincidence measurements. To enhance the light collection efficiency, a novel optical chamber has been designed. Amplifier, high-speed ADC, and FPGA are integrated into the same DMCA board. Digital signal processing, including digital filtering, trigger logic, energy calculation, and coincidence logic is realized in the FPGA within limited logic resources. The newly developed system was calibrated by multiple gamma sources as well as a voltage function generator. The excellent linearity of the system in terms of its energy response is confirmed by the calibration results. Single-channel measurements and dual-channel coincidence measurements can be switched between each other by utilizing the coincidence module that is integrated within the FPGA. This versatile functionality allows for flexible experimental setups and data acquisition strategies. Experiments were conducted using multiple gamma-ray sources and one alpha-ray source. Gamma-ray source measurements primarily for testing and calibrating the system. The results show that the new system can effectively distinguish the instrumental background from true nuclear events, and photon statistics are optimized by the contributions of two signal channels. In addition, in both gamma and alpha measurements, there is only a small difference between the count rates of the two single channels and the coincidence count rates. The entire system works correctly.

The new system is flexible in parameter adjustment and easy to cooperate with computers for data management and display. In addition, its compact design enhances portability. The FPGA technology significantly mitigates development costs and reduces power consumption. Our forthcoming objective entails the integration of the novel system into marine monitoring field applications, specifically as a pivotal component of an online marine radioactivity monitoring network. The envisioned network aims to facilitate continuous monitoring and expedite early detection of potential radioactive water contamination instances.
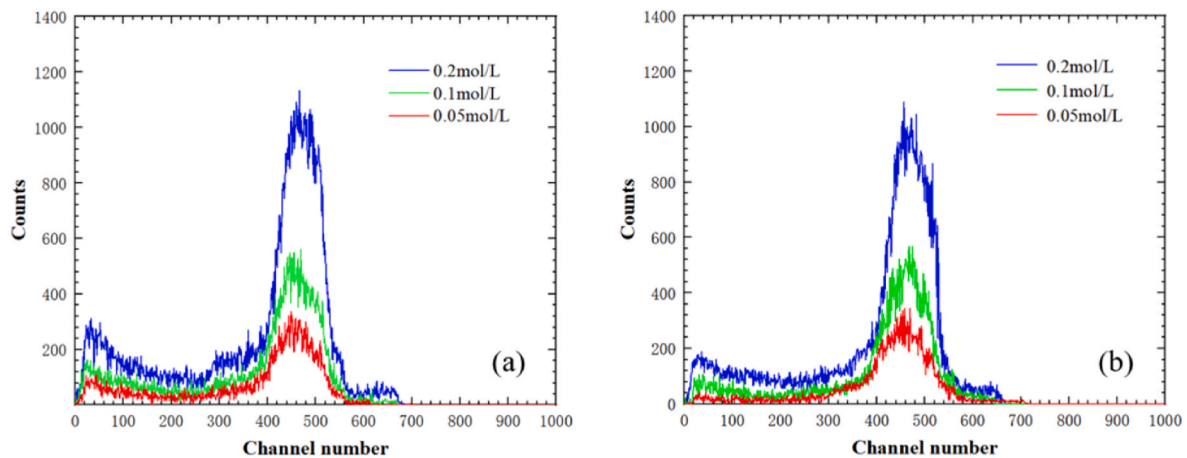
Fig. 14. Spectra of ^{232}Th. (a) Without coincidence; (b) 20ns coincidence.

Table 2
The count rate of the γ and α measurements.

Count rate/ CPS	^{137}Cs	^{22}Na	^{232}Th (0.2 mol/L)	^{232}Th (0.1 mol/L)	^{232}Th (0.05 mol/L)
Channel_A	1965	7183	799	392	208
Channel_B	1943	7159	795	391	207
30ns coincidence	1881	6956	761	372	197
20ns coincidence	1771	6669	749	362	193

Declaration of competing interest

The authors declare that they have no known competing financial interests or personal relationships that could have appeared to influence the work reported in this paper.

Data availability

Data will be made available on request.

Acknowledgments

References

[1] R. Querfeld, et al., Radionuclides in surface waters around the damaged Fukushima Daiichi NPP one month after the accident: evidence of significant tritium release into the environment, Sci. Total Environ. 689 (2019) 451–456.
[2] J.S. Chae, et al., Distribution of tritium in water vapour and precipitation around Wolsung nuclear power plant, Radiat. Protect. Dosim. 146 (2011) 330–333.
[3] M. Tayeb, et al., Rapid and simultaneous determination of Strontium-89 and Strontium-90 in seawater, J. Environ. Radioact. 153 (2016) 214–221.
[4] J.M. Pates, et al., Determination of (234)Th in marine samples by liquid scintillation spectrometry, Anal. Chem. 68 (1996) 3783–3788.
[5] C.D. Biggin, et al., Time-efficient method for the determination of Pb-210, Bi-210, and Po-210 activities in seawater using liquid scintillation spectrometry, Anal. Chem. 74 (2002) 671–677.
[6] X.L. Hou, Liquid scintillation counting for determination of radionuclides in environmental and nuclear application, J. Radioanal. Nucl. Chem. 318 (2018) 1597–1628.
[7] A.T. Susanto, et al., A systematic literature reviews of multichannel analyzer based on FPGA for gamma spectroscopy, J. Phys. Conf. 1528 (2020), 012016.
[8] R.V. Ribas, Digital pulse processing: a new paradigm for nuclear instrumentation, in: 32nd Bazilian Workshop on Nuclear Physics, Sao Paulo, BRAZIL, 2009.
[9] P.C. Tsao, et al., Nuclear pulse height measurement using FPGA techniques, in: IEEE Nuclear Science Symposium/Medical Imaging Conference, 2008. Dresden, GERMANY.
[10] E.M. Becker, A.T. Farsoni, Wireless, low-cost, FPGA-based miniature gamma ray spectrometer, Nucl. Instrum. Methods Phys. Res. Sect. A Accel. Spectrom. Detect. Assoc. Equip. 761 (2014) 99–104.
[11] A. Garcia-Duran, et al., FPGA embedded multichannel analyzer, Appl. Radiat. Isot. 141 (2018) 282–287.
[12] W.H. Zeng, The design of digital multi-channel analyzer based on FPGA, in: 3rd International Conference on Asian Nuclear Prospects (ANUP), 2012. Beijing, PEOPLES R CHINA.
[13] T. Sato, et al., Upgrades of DARWIN, a dose and spectrum monitoring system applicable to various types of radiation over wide energy ranges, Nucl. Instrum. Methods Phys. Res. Sect. A Accel. Spectrom. Detect. Assoc. Equip. 637 (2011) 149–157.
[14] W.K. Warburton, P.M. Grudberg, Current trends in developing digital signal processing electronics for semiconductor detectors, Nucl. Instrum. Methods Phys. Res. Sect. A Accel. Spectrom. Detect. Assoc. Equip. 568 (2006) 350–358.
[15] M.F. L'Annunziata, M.J. Kessler, Liquid Scintillation Analysis: Principle and Practice in Handbook of Radioactivity Analysis, Elsevier, 2012.
[16] Z.G. Ren, et al., Digital coincidence acquisition applied to portable beta liquid scintillation counting device, Nucl. Sci. Tech. 24 (2013) 47–51.
[17] S. Hurtado, GEANT4 simulation of the response of a liquid scintillation counter, J. Instrum. 12 (2017).
[18] B.E. Bernacki, et al., Optical design considerations for efficient light collection from liquid scintillation counters, Appl. Opt. 54 (2015) 2413–2423.
[19] M. Capogni, P. De Felice, A prototype of a portable TDCR system at ENEA, Appl. Radiat. Isot. 93 (2014) 45–51.
[20] Q.Q. Zhou, et al., Development of a portable TDCR system at NIM, China, Appl. Radiat. Isot. (2022) 187.
[21] R. Cherubini, et al., Gamma calibration of organic scintillators, Nucl. Instrum. Methods Phys. Res., Sect. A A281 (1989) 349–352.